



# Metastable Dendrite Morphologies in Aluminum Alloys

H. Henein<sup>1</sup> · A.-A. Bogno<sup>1</sup> · W. Hearn<sup>1</sup> · J. Valloton<sup>1</sup>

Submitted: 14 May 2020 / in revised form: 20 July 2020 / Published online: 28 August 2020  
© ASM International 2020

**Abstract** Cubic metallic alloys generally grow along  $\langle 100 \rangle$  directions due to the anisotropy of the solid–liquid interfacial energy. Under rapid solidification conditions, dendrites may deviate from  $\langle 100 \rangle$  and develop unusual morphologies. Here, Al-alloy droplets (Al-4.5Cu, Al-10Si, Al-1.9Fe, Al-33Cu, all in wt.%) were rapidly solidified using Impulse Atomization to study the microstructures forming at different cooling rates and undercoolings. Growth morphologies of Al-4.5Cu droplets were characterized using x-ray micro-tomography and EBSD. Al-dendrites were found to grow along either  $\langle 100 \rangle$  or a more unusual  $\langle 111 \rangle$  depending on the solidification conditions. Also, a transition from  $\langle 111 \rangle$  to  $\langle 100 \rangle$  in the same droplet was observed. These uncommon growth directions were also observed in other Al-alloys. In Al-1.9Fe droplets, a change in dendrite growth direction from  $\langle 100 \rangle$  to  $\langle 111 \rangle$  was observed, while  $\langle 110 \rangle$  growth directions were detected in Al-10Si samples. These experimental observations will be related to their solidification conditions using Solidification Continuous Cooling Transformation diagrams.

**Keywords** aluminum alloys · growth directions · impulse atomization · metastable

## 1 Introduction

Solidification is a complex phenomenon arising in many modern experimental techniques and industrial technologies related to casting, joining and surfaces processing. Rapid solidification of metallic alloys is an ongoing research interest in the metallurgical sphere. Such non-equilibrium processing conditions can give rise to solubility extension or the formation of metastable phases due to nucleation and/or growth kinetics, where the interface is still at local equilibrium. True departure from equilibrium of the solid–liquid interface can also be achieved, such as solute trapping where the phase diagram no longer applies for the interface and the chemical potentials are no longer equal at the interface. The variation of different conditions of solidification (such as undercooling or cooling rate) gives a possibility to control the morphology and size of crystal structure, which substantially influence physical and chemical properties of alloys.

The microstructure evolution during rapid solidification processes depends on the velocity of the solid–liquid interface, which in turn depends on the undercooling  $\Delta T$  prior to solidification of individual phases in the alloy. Undercooled melts see a large driving force for solidification created from the difference in Gibbs free energy between the solid and the metastable liquid states. Several microstructural changes have been observed in several different systems with increasing undercooling. Under certain conditions, dendrite growth deviates from  $\langle 100 \rangle$  and unusual and complex morphologies can develop. Such

---

This article is an invited paper selected from presentations at “PSDK XIV: Phase Stability and Diffusion Kinetics—Gibbs: Phase Equilibria, Diffusion and Materials Design” held during MS&T’19, September 29–October 3, 2019, in Portland, Oregon. The special sessions were dedicated to honor Dr. Patrice Turchi, recipient of the ASM International 2019 J. Willard Gibbs Phase Equilibria Award “for outstanding and pioneering contributions in the application of first-principles, quantum-mechanical calculations to the modeling of phase equilibria and thermodynamic behavior of alloys”. It has been expanded from its original presentation.

---

✉ J. Valloton  
valloton@ualberta.ca

<sup>1</sup> Department of Chemical and Materials Engineering,  
University of Alberta, Edmonton T6G 1H9, Canada

deviations were first observed during the growth of ionic crystals in aqueous solution, transparent metal analogs. Kahlweit et al. highlighted the growth orientation change of  $\text{NH}_4\text{Cl-H}_2\text{O}$  crystals from  $\langle 100 \rangle$  to  $\langle 110 \rangle$  and then  $\langle 111 \rangle$  with increasing growth velocity.<sup>[1]</sup> The authors investigated the growth orientation during isothermal solidification by varying the nucleation undercooling through changes in supersaturation and solidification temperature. In a subsequent investigation of this system, Chan et al. suggested that at low undercoolings, the growth orientation is imposed by the anisotropy of interfacial free energy, with a transition from  $\langle 100 \rangle$  to  $\langle 110 \rangle$  observed as the supersaturation increases.<sup>[2]</sup> At high undercoolings, the growth of  $\langle 111 \rangle$  dendrite is attributed to the “anisotropy of rate constant”, i.e. attachment kinetics. Further studies into the  $\text{NH}_4\text{Cl-H}_2\text{O}$  system by directional solidification showed oscillations between these different growth modes and the velocity range over which they occur correlates well with the isothermal experiments of Kahlweit.<sup>[3]</sup>

Unusual dendrite growth morphologies have also been observed in aluminium alloys. Herenguel first reported twinned dendrites, or so-called feathery grains in semi-continuous castings<sup>[4]</sup>. Using Electron BackScattered Diffraction (EBSD), Henry et al. showed that feathery grains in Al-Mg-Si, Al-Si-Ti and Al-Cu cast billets were made of  $\langle 110 \rangle$  dendrites with their trunk split by a  $\{111\}$  twin plane.<sup>[5]</sup> Using a Bridgman type directional solidification and a unidirectional solidification setup, Henry et al. obtained other morphologies dependent on the alloy composition, growth velocity and temperature gradient.<sup>[6]</sup> For instance, so-called degenerate feathery grains were observed in Al-9 wt.%Si. These non-twinned dendrite morphologies grow along  $\langle 110 \rangle$  with secondary arms of  $\langle 100 \rangle$  and  $\langle 110 \rangle$  types.

Sémoroz et al. studied dendrite formation in Al-45 wt.%Zn coating on hot-dipped steel sheets.<sup>[7]</sup> They observed an eight-fold symmetry dendritic pattern in grains having a (001) plane parallel to the surface. Their EBSD analysis unambiguously identified these as  $\langle 320 \rangle$  dendrite growth directions. These observations have been further analyzed in Al-Zn alloys by Gonzales et al. using directional solidification and Bridgman solidification over a wide range of compositions.<sup>[8]</sup>  $\langle 100 \rangle$  dendrites were found for compositions up to 25 wt.%Zn while  $\langle 110 \rangle$  growth directions were seen above 65 wt.%Zn. In between these two compositions, a continuous change of growth direction from  $\langle 100 \rangle$  to  $\langle 110 \rangle$  was highlighted. This so-called Dendrite Orientation Transition (DOT) was then successfully simulated by Haxhimali et al. using the phase field method.<sup>[9]</sup> The origin of the DOT has been attributed to a change in the solid–liquid interfacial energy anisotropy.<sup>[10]</sup>

More recently, the origin of twinned dendrites in Al alloys has been identified in the same Al-Zn alloys as

coming from icosahedral short-range order in the liquid,<sup>[11]</sup> when very small amount of Cr is added. This leads to quasicrystal formation from which the fcc phase grows with epitaxial relationships leading to multiple twinning relationships of grains.

Becker et al. observed a DOT similar to that of Al-Zn in the Al-Ge system by conducting isothermal solidification experiments in thin samples under slow cooling conditions.<sup>[12]</sup> Primary dendrite arms are growing along  $\langle 100 \rangle$  in Al-20 wt.%Ge alloys, along  $\langle 110 \rangle$  in Al-46 wt.%Ge, while both directions are growing simultaneously at an intermediate composition of Al-29 wt.%Ge. These microstructures were successfully modelled using phase-field simulations with varying solid–liquid interfacial energy anisotropies.<sup>[12]</sup>

Lately, Wang et al. examined the change in dendrite growth direction in laser-melted Al-Sm alloys as a function of samarium content.<sup>[13]</sup> A transition from  $\langle 100 \rangle$  to seaweed was observed at  $\sim 2.2$  at.% Sm, and to  $\langle 110 \rangle$  at  $\sim 5.6$  at.% Sm, which is again attributed to changes in the interfacial free energy anisotropy induced by the solute. This was confirmed using Molecular Dynamic simulations to calculate the two parameters used to characterize the anisotropy,  $\epsilon_1$  (fourfold symmetric contribution) and  $\epsilon_2$  (sixfold contribution). A clear variation in the ( $\epsilon_1$ ,  $-\epsilon_2$ ) space is predicted as the Sm content increases. The interfacial anisotropy changes such that the expected dendritic growth directions shift from  $\langle 100 \rangle$  to seaweed to  $\langle 110 \rangle$ .

All these experiments suggest that the transition to  $\langle 110 \rangle$  is induced by the variation of interfacial energy anisotropy, while attachment kinetics would explain the change to  $\langle 111 \rangle$  orientation seen with increasing solidification rate.

More than twenty-five techniques have been reported to induce rapid solidification,<sup>[14]</sup> the most widely used being atomization. Impulse Atomization (IA) is a single fluid atomization technique that yield droplet solidification with large levels of undercooling over a wide range of cooling rates.<sup>[15,16]</sup> This paper compiles new and previously reported occurrences of metastable dendrite morphologies observed in rapidly solidified Al-based alloys obtained by IA. The aim is to explore common features in morphology in various hypoeutectic Al alloys, namely Al-Cu, Al-Si, Al-Fe, Al-Zn, Al-Ge, as well as near-eutectic Al-Cu.

## 2 Experimental methods

Impulse atomization (IA) (a type of drop tube) is a containerless solidification technique (Fig. 1). It consists in the transformation of a bulk liquid into a spray of liquid droplets. A plunger (or impulse applicator) applies a pressure (or impulse) to the melt in order to push it through a nozzle plate with several orifices of known size and geometry.

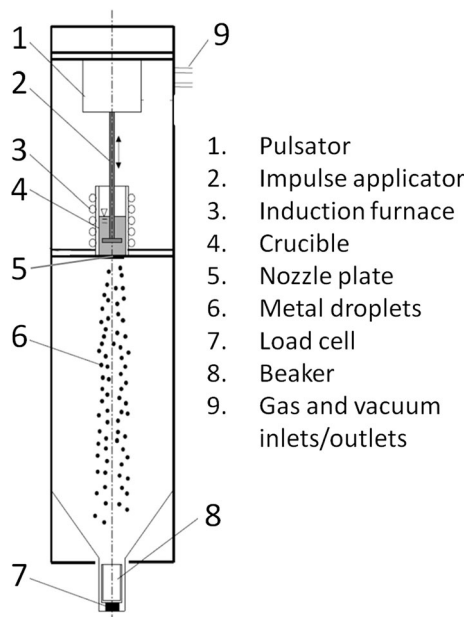


**Fig. 1** Schematic view of an impulse atomization apparatus

Liquid ligaments emanate from each orifice, which in turn break up into droplets. Rapid solidification of the droplets then occurs during free fall by heat loss to the surrounding gas (usually He, N<sub>2</sub> or Ar). The thermal history of the liquid droplets is a function of both the droplet size and the gas in the atomization tower and has been described mathematically by previous workers.<sup>[17,18]</sup> The solidified samples can finally be collected at the bottom of the tower and subsequently sieved into different size classes. A detailed description of the process is available in Ref. 15.

### 3 Results and Discussion

An in-depth study of Impulse Atomized Al-4.5 wt.%Cu was carried out by Bedel et al.<sup>[19]</sup> This alloy is widely used as a model for solidification studies and its thermophysical properties are well documented. Two sets of droplets were atomized using different gas atmospheres, helium and argon. Post-mortem synchrotron x-ray micro-tomography was carried out on these droplets at ESRF (European Synchrotron Radiation Facility, Grenoble, France). Careful analysis of more than 200 particles revealed four main distinct dendritic morphologies (Fig. 2). The highly branched morphology (a) shows dendrites growing with a four-fold symmetry typical of  $\langle 100 \rangle$  growth while microstructural features indicate that dendrite arms develop mostly along  $\langle 111 \rangle$  directions in the other three morphologies (b–d).

The assumed growth directions from the tomography analysis have been confirmed using EBSD on selected

droplets. Figure 3 (left) shows the cross section of a 960  $\mu\text{m}$  droplet atomized in argon exhibiting the highly branched morphology along with its corresponding pole figures. This cross section lies in a  $\{001\}$  plane. The primary dendrite trunk directions, highlighted by the red arrows, correspond to the  $\langle 100 \rangle$  poles. Microtomography cross sections along the XZ and YZ planes (i.e. after a 90° rotation around the X or Y axis of this particular cross section) exhibit a similar morphology, suggesting that the dendritic microstructure developed along  $\langle 100 \rangle$  throughout the whole droplet. Figure 3 (right) shows the cross section and pole figures of a 415  $\mu\text{m}$  particle atomized in helium with the finger bundle structure. This particular cut lies this time in a  $\{011\}$  plane. Two of the four  $\langle 111 \rangle$  poles are well aligned with the bundles, as shown by the blue arrows. This is consistent with a  $\langle 111 \rangle$  dendritic growth.

Only 7.8% of all the droplets analyzed solidified completely along  $\langle 100 \rangle$  directions. The majority of droplets showed at least some instances of  $\langle 111 \rangle$  growth. The transition from  $\langle 100 \rangle$  to  $\langle 111 \rangle$  is attributed to the variation of the attachment kinetics anisotropy as the solidification growth velocity increases.  $\langle 100 \rangle$  arms develop at low solidification growth velocity (Fig. 2a). As the cooling rate and/or undercooling increases, primary arms start growing along  $\langle 111 \rangle$ . However, growth reverts to  $\langle 100 \rangle$  for slower growing side arms formed after recalescence (Fig. 2b). At even higher solidification rates, the droplet solidifies completely with a  $\langle 111 \rangle$  growth direction, as illustrated in Fig. 2c. Finally, at the highest speed, finger bundles stem from a growth competition between different  $\langle 111 \rangle$  dendrites originating from the same nucleation point (Fig. 2d). The  $\langle 111 \rangle$  dendritic structure is found again in regions of the droplet with slower solidification velocity. The distribution of the four observed morphologies was established by careful analysis of a large number of droplets solidified in argon from two size categories (73 droplets with a diameter smaller than 212  $\mu\text{m}$  and 64 droplets between 250 and 300  $\mu\text{m}$ , Fig. 4). Due to the stochastic nature of nucleation, all morphologies are found within a single size range. However, growth directions tend to shift towards the faster  $\langle 111 \rangle$  morphologies when the droplet size decreases. Indeed, when the droplets are smaller, they solidify faster due to the larger surface to volume ratio. The same trend is observed when switching the gas atmosphere. For a given size range, the morphology is more often of the finger-bundle type in droplets solidified in helium, due to its higher thermal conductivity and hence higher cooling rates.

Subsequent work on the rapid solidification of Al-4.5 wt.%Cu and Al-4.5 wt.%Cu-0.4 wt.%Sc estimated the undercooling temperatures of both the primary phase and the eutectic structures in these alloys.<sup>[20]</sup> In order to represent the resultant microstructure and relate it to macro-solidification conditions, Solidification Continuous Cooling

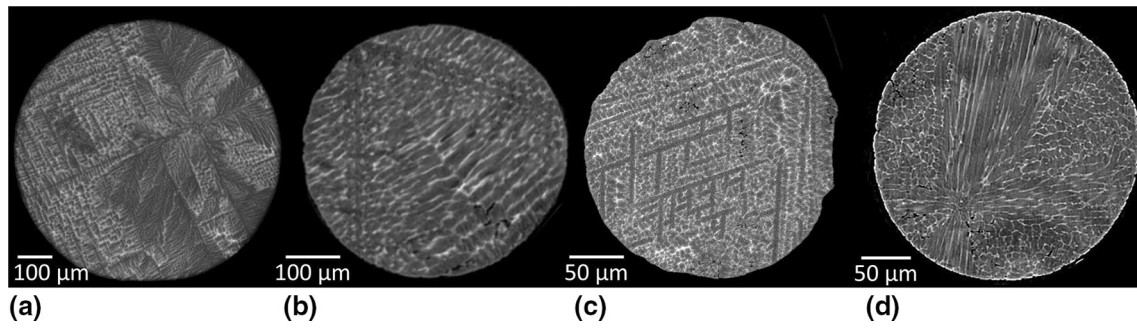


**Fig. 2** Synchrotron x-ray tomography images depicting the four typical dendrite morphologies observed in Al-4.5 wt%Cu droplets solidified in IA: (a)  $\langle 100 \rangle$  highly branched dendrites; (b)  $\langle 111 \rangle$  to  $\langle 100 \rangle$  dendrite transition; (c)  $\langle 111 \rangle$  dendritic morphology; (d)  $\langle 111 \rangle$  finger bundle morphology. The black rings are reconstruction artifacts

**Fig. 3** Left: 960  $\mu\text{m}$  Al-4.5 wt%Cu particle atomized in Ar and EBSD pole figures for  $\alpha\text{-Al}$  showing the  $\langle 100 \rangle$  growth of the highly branched morphology; Right: 415  $\mu\text{m}$  Al-4.5 wt%Cu particle atomized in He and EBSD pole figures for  $\alpha\text{-Al}$  showing the  $\langle 111 \rangle$  growth of the finger bundle morphology

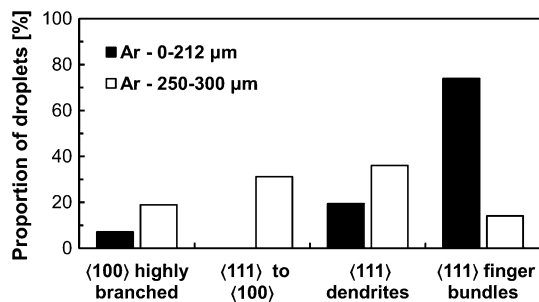
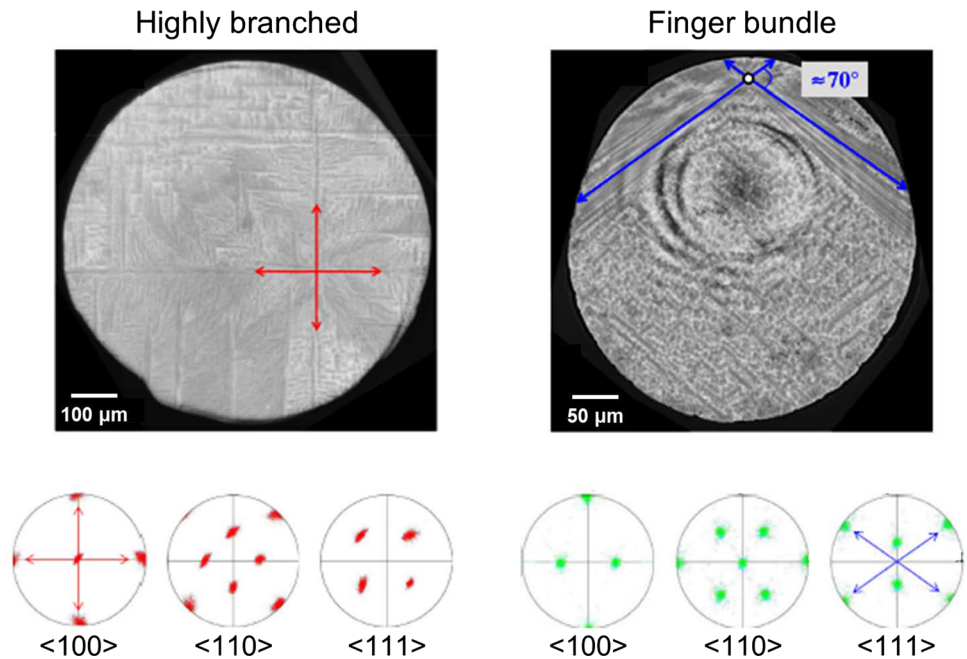


**Fig. 4** Distribution of the four morphologies in Al-4.5 wt%Cu droplets solidified in argon for two diameter ranges (73 droplets for  $0 < d < 212 \mu\text{m}$  and 64 droplets for  $250 \mu\text{m} < d < 300 \mu\text{m}$ )

Transformation (SCCT) diagrams were developed.<sup>[20]</sup> To construct these maps, the liquid cooling rates of the samples are used and the corresponding undercoolings are

plotted on a CCT diagram (Fig. 5). Also plotted on this graph are the equilibrium liquidus and eutectic temperatures,  $T_L$  and  $T_E$  respectively. Finally, the resulting proportions of droplets exhibiting any type of  $\langle 111 \rangle$  growth ( $\langle 111 \rangle$  to  $\langle 100 \rangle$  transition,  $\langle 111 \rangle$  dendrites and finger bundles) are also indicated for each cooling rate. Over the range studied, primary nucleation undercoolings are high, starting at 60 K at 500 K/s and steadily increasing up to 86 K at 30,000 K/s. Dendrites growing along  $\langle 111 \rangle$  can be found under all solidification conditions analyzed and are the predominant morphology at all but the lowest cooling rate. In addition, samples processed under lower cooling rates ( $\sim 10\text{--}50 \text{ K/s}$ ) and undercoolings ( $\sim 5\text{--}45 \text{ K}$ ) using electromagnetic levitation only showed dendrites growing along  $\langle 100 \rangle$ <sup>[20]</sup>. This clearly indicates that the transition from  $\langle 100 \rangle$  to  $\langle 111 \rangle$  is related to the solidification conditions and supports the hypothesis that the variation of the

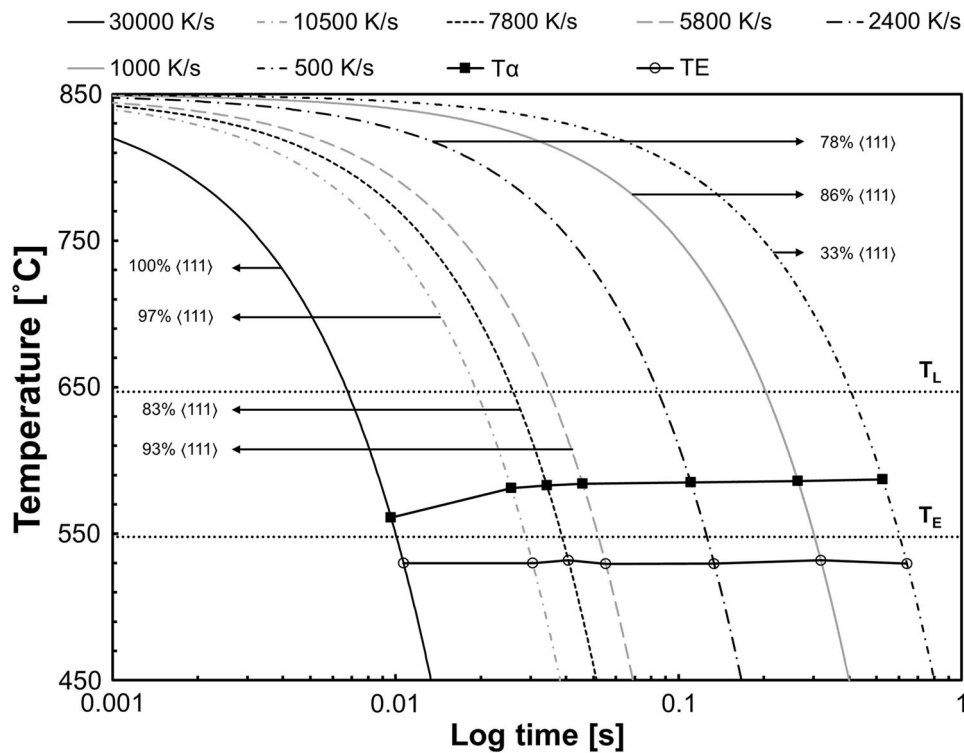
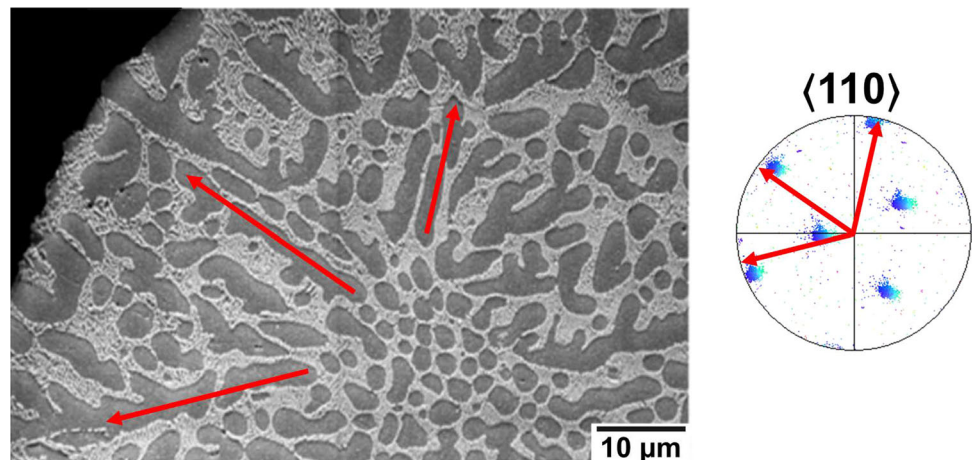


**Fig. 5** Solidification Continuous Cooling Transformation curves of Impulse Atomized Al-4.5 wt%Cu

**Fig. 6** 230  $\mu\text{m}$  Al-10 wt%Si particle atomized in He. (left): SEM micrograph; (right):  $\alpha$ -Al  $\langle 110 \rangle$  pole figure



attachment kinetics anisotropy is responsible for the observed transition.

Unusual growth directions were also observed in atomized Al-10 wt.%Si droplets. One such example is shown in Fig. 6.<sup>[21]</sup> In this 230  $\mu\text{m}$  particle atomized in He, the primary  $\alpha$ -Al shows a clear 6-fold symmetry. EBSD analysis shows that the whole particle is constituted of a single  $\alpha$ -Al grain, while the pole figure clearly indicates  $\langle 110 \rangle$  growth directions.

Figure 7 shows the proportion of droplets exhibiting  $\langle 110 \rangle$  growth. While it was not observed in droplets

solidified in argon, this  $\langle 110 \rangle$  growth only occurred in the finer particle sizes that were atomized in helium. This indicates that this growth mode is dependent on solidification conditions, i.e. cooling rate and/or nucleation undercooling. However, it is different from the  $\langle 111 \rangle$  observed in Al-Cu and Al-Fe alloys. As mentioned above,  $\langle 110 \rangle$  growth was reported in Al-Si and Al-Ge alloys (Ge and Si having many similar properties). The Al-Ge results were obtained at very low solidification rate, with this transition clearly attributed to changes in the surface energy anisotropy with increasing solute content.<sup>[12]</sup>  $\langle 110 \rangle$

growth in unidirectionally solidified Al-9 wt.%Si was however obtained at a much higher solidification rate<sup>[6]</sup>. While kinetics effects cannot totally be discounted for this particular transition, it is possible that rapid solidification induces  $\langle 110 \rangle$  growth by increasing the supersaturation, which could change the surface energy anisotropy in favor of  $\langle 110 \rangle$ .

A seaweed-type of growth was also observed in many Al-10 wt.%Si droplets, as shown in Fig. 8. This seaweed morphology is characterized by a highly branched structure that grows outwards from the primary arms at an angle below 90°. During seaweed growth, the growing dendrites bend away from the primary arm and split, causing them to grow in a “zig-zag” fashion.

Seaweed structures were observed by Friedli et al. in Al-Zn alloys directionally solidified at low growth velocities.<sup>[10]</sup> The zigzagging of the arms was considered a response to perturbations at the solidification front, caused by the solute field of another arm. The rejected solute changes the surface tension anisotropy at the solidification front, which forces the growing  $\alpha$ -Al dendrite to bend,

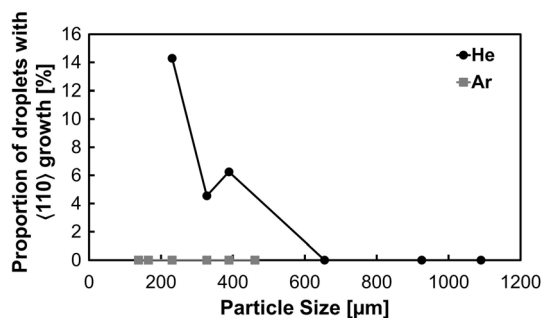


**Fig. 7** Proportion of Al-10 wt%Si powders exhibiting  $\langle 110 \rangle$  growth directions as a function of particle size and atomization gas

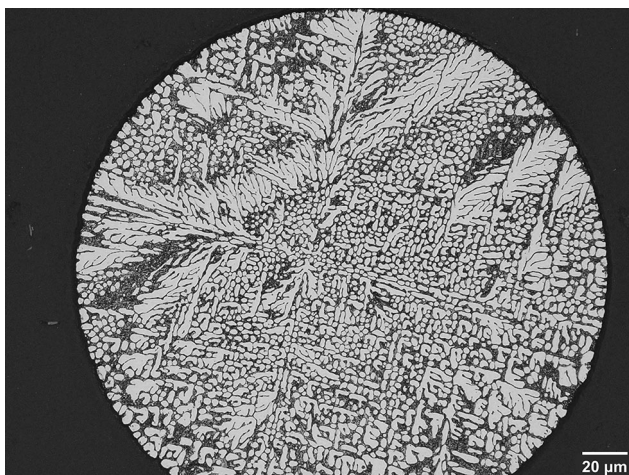


**Fig. 8** Optical micrograph outlining the seaweed growth of  $\alpha$ -Al phase in a 212–250  $\mu\text{m}$  Al-10 wt%Si droplet atomized in helium

switch sides and form a seaweed structure. Hence, solute effects play a role in the Al-Zn alloys. It remains unclear how segregation and undercooling interplay between solute and kinetic effects.

Using the phase-field method to model the solidification of pure metallic melts, Mullis et al. highlighted a transition to seaweed growth with increasing undercoolings.<sup>[22]</sup> As undercooling increases, the dendrite growth velocity would also increase and promote the onset of dendrite tip splitting. Furthermore, an increase in growth velocity causes the initial side-branching to move closer to the dendrite tip. Mullis et al. considered this shift in the perturbations at the solidification front to be a competition between the surface tension anisotropy and the atom attachment kinetics, where the influence of kinetics became more dominant at higher growth velocities. Experimental work done by Assadi et al.<sup>[23]</sup> with  $\text{Ni}_{51}\text{Al}_{49}$  alloys found that at higher growth velocities seaweed growth was possible, where the formation of the seaweed structure was also attributed to the increasing role of atom attachment kinetics.

To relate the solidification conditions to the seaweed growth observed in Al-10 wt%Si, a visual analysis was conducted to determine the number of powders, within a particle size range, that displayed seaweed growth (Fig. 9). Experimental conditions noticeably influence the growth of the seaweed structure. Decreasing the particle size and using helium (instead of argon) will make seaweed growth more prevalent. These results indicate that seaweed growth in atomized Al-10 wt%Si might be caused by the increasing role of atom attachment kinetics, due to an increase in the  $\alpha$ -Al dendrite growth velocity.

Similarly, to Al-4.5 wt%Cu, an SCCT diagram was developed. This combines the above results and outlines the solidification pathway of Impulse Atomized Al-10 wt%Si droplets (Fig. 10). This plot clearly shows that the metastable morphologies, be it seaweed structures or dendrites growing along  $\langle 110 \rangle$ , are favored by high cooling rates and undercoolings. This again indicates that the prevalence of metastable morphologies is related to solidification conditions. While attachment kinetics effects are

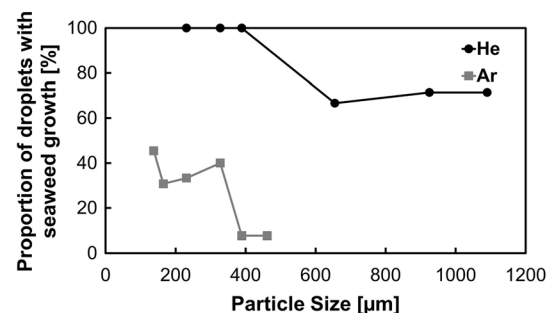


**Fig. 9** Proportion of Al-10 wt%Si powders exhibiting seaweed-type growth as a function of particle size and atomization gas

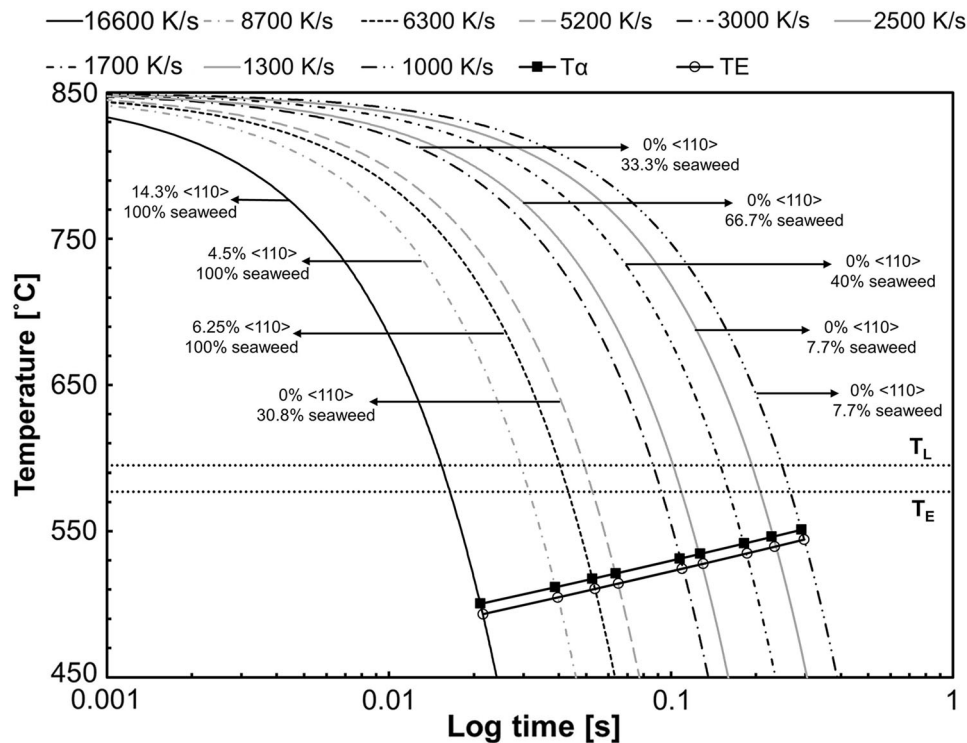


**Fig. 10** Solidification Continuous Cooling Transformation curves of Impulse Atomized Al-10 wt%Si

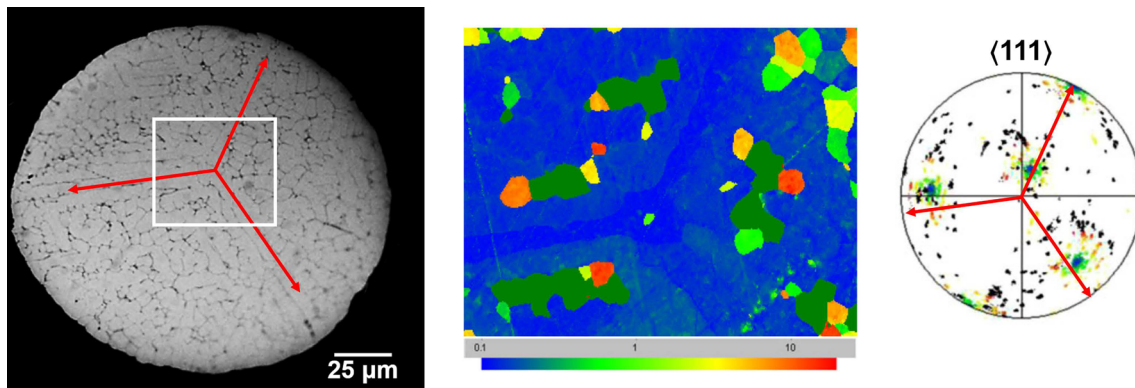


**Fig. 11** 355  $\mu\text{m}$  Al-0.61 wt%Fe particle atomized in He. (left): optical; (middle): EBSD false color reconstruction; (right):  $\alpha\text{-Al}$   $\langle 111 \rangle$  pole figure

likely responsible for the formation of seaweed, the exact reason for the transition to  $\langle 110 \rangle$  remains unclear.

The microstructure evolution of impulse atomized powders of Al-0.61 wt%Fe has been investigated by Henein et al.<sup>[24]</sup> and Chen et al.<sup>[25]</sup> The solidification cooling rate of a 355  $\mu\text{m}$  droplet of Al-0.6 wt.%Fe atomized in helium was reported as about 4000 K/s. Figure 11 shows an optical image of a 355  $\mu\text{m}$  droplet atomized in He. Primary trunks are extending in three different directions from a single nucleation site. EBSD analysis around the nucleation site was performed (Fig. 11). On this

reconstructed map, the orientation of the nucleation center was chosen as a reference. The false coloring corresponds to the misorientation angle from the nucleation center. The color scheme shows that misorientation for most of the region, especially the three main trunks, is within 1 degree. While no clear side arms can be seen, it is apparent that the growth direction of the primary trunks coincide with the three outer poles of the  $\langle 111 \rangle$  pole figure. The misorientation of the side arms is attributed to fragmentation. Local remelting and break-off of dendrite arms takes place in the mushy zone during recalescence.<sup>[26]</sup> Fragments that do not

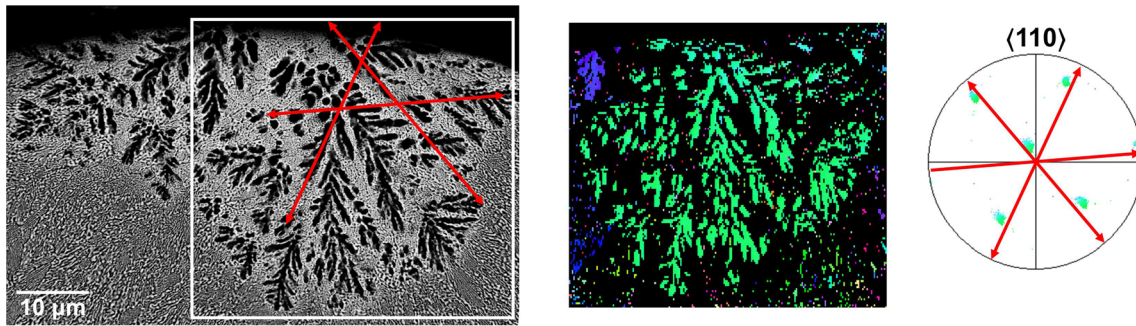


**Fig. 12** 275  $\mu\text{m}$  Al-33 wt%Cu particle atomized in Ar. (left): SEM micrograph; (middle): EBSD false color reconstruction; (right):  $\langle 110 \rangle$  pole figure

fully melt can grow further, forming new grains. As the free-falling droplets are almost devoid of convection, their orientation would not deviate greatly from the parent dendrite. Thus, no major misorientation is observed.

Another instance of deviation from  $\langle 100 \rangle$  growth has been observed when atomizing an Al-Cu melt of eutectic composition (Al-33 wt%Cu). While the vast majority of droplets exhibited a fully eutectic microstructure, some droplets showed nucleation of  $\alpha$ -Al dendrites prior to eutectic solidification. This indicates that the melt composition was somehow locally hypo-eutectic. An example is shown in Fig. 12. It is clear that the dendrite arms do not grow at  $90^\circ$  from each other, indicating a growth direction different from  $\langle 100 \rangle$ . EBSD mapping of this sample shows that two different nucleation events happened. The  $\alpha$ -Al dendrites on the left being part of one grain (blue) and the ones on the right constituting a second grain (green). Looking at the pole figure, it appears that the dendrites are growing along  $\langle 110 \rangle$ . This is most intriguing as both aluminum and copper are FCC crystals with interfacial energy anisotropies favoring  $\langle 100 \rangle$  growth.

## 4 Conclusions

Al-alloy droplets of various compositions were rapidly solidified using Impulse Atomization to study the microstructures forming at different cooling rates and undercoolings. Deviation from the usual  $\langle 100 \rangle$  growth direction was observed. In Al-4.5 wt.%Cu and Al-0.61 wt.%Fe, dendrites can grow along  $\langle 111 \rangle$  depending on the solidification conditions. Higher cooling rates and/or undercooling favour a transition to  $\langle 111 \rangle$ . This suggests that anisotropy of attachment kinetics is a contributing factor, as observed in transparent alloys.  $\langle 110 \rangle$  growth directions were detected in Al-10 wt.%Si, with occurrences increasing with the solidification rate. While attachment kinetics cannot be discarded, it is usually linked to  $\langle 111 \rangle$

growth. Germanium, which has similar properties to silicon, was shown to induce a DOT in Al-Ge alloys. Thus it is suggested that rapid solidification conditions might locally change the interfacial energy anisotropy with increasing supersaturation. The presence of  $\langle 110 \rangle$   $\alpha$ -Al in near eutectic Al-Cu is still puzzling, as both elements have anisotropies that favour  $\langle 100 \rangle$  growth.

**Acknowledgment** Financial support from the Natural Sciences and Engineering Research Council of Canada (NSERC), the Holistic Innovation in Additive Manufacturing (HI-AM) Network and the European Space Agency (ESA) within the frame of the NEQUISOL project is gratefully acknowledged. The assistance of Daniel Auras with morphology analysis is appreciated.

## References

1. M. Kahlweit, On the Dendritic Growth of  $\text{NH}_4\text{Cl}$ , Crystals from Aqueous Solutions. II, *J. Cryst. Growth*, 1970, **7**, p 74-78
2. S.-K. Chan, H.-H. Reimer, and M. Kahlweit, On the Stationary Growth Shapes of  $\text{NH}_4\text{Cl}$  Dendrites, *J. Cryst. Growth*, 1976, **32**, p 303-315
3. K.A. Gudgel and K.A. Jackson, Oscillatory Growth of Directionally Solidified Ammonium Chloride Dendrites, *J. Cryst. Growth*, 2001, **225**, p 264-267
4. J. Herenguel, Les procédés de coulée semi-continue et continue des métaux non ferreux et leurs conséquences métallurgiques, *Revue de Métallurgie*, 1948, **45**, p 139-146
5. S. Henry, P. Jarry, and M. Rappaz,  $\langle 110 \rangle$  Dendrite Growth in Aluminum Feathery Grains, *Metall. Mater. Trans. A*, 1998, **29**, p 2807-2817
6. S. Henry, T. Minghetti, and M. Rappaz, Dendrite Growth Morphologies in Aluminium Alloys, *Acta Mater.*, 1998, **46**(18), p 6431-6443
7. A. Sémoroz, Y. Durandet, and M. Rappaz, EBSD Characterization of Dendrite Growth Directions, Texture and Misorientations in Hot-Dipped Al-Zn-Si Coatings, *Acta Mater.*, 2001, **49**, p 529-541
8. F. Gonzales and M. Rappaz, Dendrite Growth Directions in Aluminum-Zinc Alloys, *Metall. Mater. Trans. A*, 2006, **37**, p 2797-2806
9. T. Haxhimali, A. Karma, F. Gonzales, and M. Rappaz, Orientation Selection in Dendritic Evolution, *Nat. Mater.*, 2006, **5**, p 660-664



10. J. Friedli, J.L. Fife, P. Di Napoli, and M. Rappaz, Dendritic Growth Morphologies in Al-Zn Alloys—Part I: X-ray Tomographic Microscopy, *Metall. Mater. Trans. A*, 2013, **44**, p 5522-5531
11. G. Kurtuldu, P. Jarry, and M. Rappaz, Influence of Icosahedral Short Range Order on Diffusion in Liquids: A Study on Al-Zn-Cr Alloys, *Acta Mater.*, 2016, **115**, p 423-433
12. M. Becker, J.A. Dantzig, M. Kolbe, S.T. Wiese, and F. Kargl, Dendrite Orientation Transition in AlGe Alloys, *Acta Mater.*, 2019, **165**, p 666-677
13. L. Wang, J. Hoyt, N. Wang, N. Provatas, and C.W. Sinclair, Controlling Solid-Liquid Interfacial Energy Anisotropy Through the Isotropic Liquid, *Nat. Commun.*, 2020, **11**, p 724
14. S.J. Savage and F.H. Froes, Production of Rapidly Solidified Metals and Alloys, *J. Metals*, 1984, **36**(4), p 20-32
15. H. Henein, Single Fluid Atomization Through the Application of Impulses to a Melt, *Mater. Sci. Eng. A*, 2002, **326**(1), p 92-100
16. N. Ellendt, R. Schmidt, J. Knabe, H. Henein, and V. Uhlenwinkel, Spray Deposition Using Impulse Atomization Technique, *Mater. Sci. Eng. A*, 2004, **383**(1), p 107-113
17. J.B. Wiskel, H. Henein, and E. Maire, Solidification Study of Aluminum Alloys Using Impulse Atomization: Part I: Heat Transfer Analysis of an Atomized Droplet, *Can. Metall. Quart.*, 2002, **41**(1), p 97-110
18. J.B. Wiskel, H. Henein, and E. Maire, Solidification Study of Aluminum Alloys Using Impulse Atomization: Part II: Effect of Cooling Rate on Microstructure, *Can. Metall. Q.*, 2002, **41**(2), p 193-204
19. M. Bedel, G. Reinhart, A.-A. Bogno, C.-A.J.S. Gandin, E. Boller, H. Nguyen-Thi, and H. Henein, Characterization of Dendrite Morphologies in Rapidly Solidified Al-4.5 wt.%Cu Droplets, *Acta Mater.*, 2015, **89**, p 234-246
20. J. Valloton, A.-A. Bogno, H. Henein, D.M. Herlach, and D. Sediako, Scandium Effect on Undercooling and Dendrite, *Metall. Mater. Trans. A*, 2019, **50**, p 5700-5706
21. W. Hearn, *The Microstructure, Morphology and Mechanical Properties of Rapidly Solidified Al-10 wt.%Si Alloy*, University of Alberta, Edmonton, 2018
22. A. Mullis, K. Dragnevski, and R. Cochrane, The Transition from the Dendrite to the Seaweed Growth Morphology During the Solidification of Deeply Undercooled Metallic Melts, *Mater. Sci. Eng. A*, 2004, **375–377**, p 157-162
23. H. Assadi, M. Oghabi, and D.M. Herlach, Influence of Ordering Kinetics on Dendritic Growth Morphology, *Acta Mater.*, 2009, **57**, p 1639-1647
24. H. Henein, V. Buchoud, R.-R. Schmidt, C. Watt, D. Malakov, C.-A. Gandin, G. Lesoult, and V. Uhlenwinkel, Droplet Solidification of Impulse Atomized Al-0.61Fe and Al-1.9Fe, *Can. Metall. Quart.*, 2010, **49**(3), p 275-292
25. J. Chen, U. Dahlborg, C.M. Bao, M. Calvo-Dahlborg, and H. Henein, Microstructure Evolution of Atomized Al- 0.61 wt%Fe and Al-1.90 wt%Fe Alloys, *Metall. Mater. Trans. B*, 2011, **42**, p 557-567
26. R. Heringer, C.-A. Gandin, G. Lesoult, and H. Henein, Atomized Droplet Solidification as an Equiaxed Growth Model, *Acta Mater.*, 2006, **54**, p 4427-4440

**Publisher's Note** Springer Nature remains neutral with regard to jurisdictional claims in published maps and institutional affiliations.